Journal of Solid State Chemistry 213 (2014) 268–274

Contents lists available at ScienceDirect

Journal of Solid State Chemistry

journal homepage: www.elsevier.com/locate/jssc

Structural, electrochemical and magnetic characterization of the layered-type $PrBa_{0.5}Sr_{0.5}Co_2O_{5+\delta}$ perovskite

Abul K. Azad [a,b,*], Jung H. Kim [c], John T.S. Irvine [a]

[a] School of Chemistry, University of St Andrews, Fife KY16 9ST, UK
[b] Faculty of Integrated Technologies, Universiti Brunei Darussalam, Gadong BE 1410, Brunei Darussalam
[c] Department of Applied Materials Science and Engineering, Hanbat National University, San 16-1, Dukmyung-Dong, Yusung-Gu, Daejeon 305-719, South Korea

ARTICLE INFO

Article history:
Received 8 October 2013
Received in revised form
5 March 2014
Accepted 6 March 2014
Available online 15 March 2014

Keywords:
Perovskite
Solid solution
Structure
Neutron powder diffraction
Magnetic properties

ABSTRACT

Structural, electrical and magnetic properties of the layered cobaltite $PrBa_{0.5}Sr_{0.5}Co_2O_{5+\delta}$ have been investigated by means of neutron diffraction, electron diffraction, thermogravimetric analysis and SQUID magnetometry. Rietveld analysis of neutron diffraction data shows the ordered distribution of oxygen vacancies in $[PrO_\delta]$ planes which doubles the lattice parameters from the simple perovskite cell parameter as $a \approx 2a_p$ and $c \approx 2a_p$ (a_p is the cell parameter of the simple Perovskite) yielding tetragonal symmetry in the *P4/mmm* space group. On heating, above 573 K in air, structural rearrangement takes place and the structure can be defined as $a \approx a_p$ and $c \approx 2a_p$ in the same space group. Oxygen occupancies have been determined as a function of temperature from neutron diffraction results. Initially ($\geq$373 K), oxygen occupancy was increased and then decreased with increasing temperature. It was found that at 973 K the total oxygen loss is calculated about 0.265 oxygen/formula unit. Oxygen vacancy ordering was observed below 573 K, and the oxygen occupancy decreases as cell volume increases with increasing temperature. Area specific resistance (ASR) measurements show a resistance of 0.153 Ωcm^2 and 0.286 Ωcm^2 at 973 K and 923 K, respectively. On cooling, paramagnetic to ferromagnetic and an incomplete ferromagnetic to antiferromagnetic transition takes place. Different behaviours in field cooled and zero-field-cooled measurements leads to a coexistence of ferromagnetic and antiferromagnetic order.

1. Introduction

Cobalt containing perovskite oxides have superior oxygen activation kinetics and show unique electronic and magnetic properties as a consequence of the ability of Co to adopt 2+, 3+ and 4+ oxidation states [1–3]. In addition to the spin, charge and orbital degrees of freedom found in the manganite perovskites, the cobaltates are expected to exhibit a degree of freedom in the electronic configuration of the cobalt ion. Layered cobaltites with general formula $LnBaCo_2O_{5+\delta}$ (*Ln*=lanthanides, $0<\delta<1$) have been the subject of several studies during the last years due to their giant magnetoresistance (the highest found in cobalt oxides), the spin-state transitions, the interplay of the spin-state with the charge, orbital and metal-insulator transitions [4–9]. More recently, these materials have been found to be good cathode materials for solid oxide fuel cells [10–12]. The oxygen content and mobility plays the major role for their electronic, magnetic and transport properties. The oxygen content also controls the mean valence of Co ions, the coordination of Co (pyramidal or octahedral) and has a strong influence on the spin state of cobalt. So far, most of the investigations have concentrated on two particular compositions, namely δ=0.0 and 0.5, for which an ordering of oxygen vacancies possibly exists. In $LnBaCo_2O_5$ (δ=0) the pyramidal positions are occupied by the same amount of Co^{2+} and Co^{3+} ions. In contrast, in $LnBaCo_2O_{5.5}$ (δ=0.5) only Co^{3+} ions are present which coexist in ideally alternating octahedral CoO_6 and pyramidal CoO_5 environments. For low δ, there is a strong tendency to form charge-ordered structures which has been reported for $YBaCo_2O_5$ [4] and $TbBaCo_2O_5$ [5]. Defect equilibrium in $PrBaCo_2O_{5+d}$ at elevated temperatures has been studied by Suntsov et al. [13]. Neutron diffraction measurements show that $LnBaCo_2O_5$ (δ=0) compounds are antiferromagnetic (AFM) with T_N ~350 K (for *Y*) [14], ~380 K (*Ln*=Nd) [15]. Metal-insulator and spin-state transitions as well as successive magnetic transitions due to competing ferromagnetic (FM)–AFM interactions are present in compounds with δ=0.5 for a wide variety of rare earths [1,6,9,16]. The metal-insulator transition mainly takes place in the

* Corresponding author at: Faculty of Integrated Technologies, Universiti Brunei Darussalam, Jalan Tunku Link, Gadong BE 1410, Brunei Darussalam. Tel.: +673 725 7754.
E-mail address: abul.azad@ubd.edu.bn (A.K. Azad).

http://dx.doi.org/10.1016/j.jssc.2014.03.008
0022-4596/

temperature range from room temperature to 373 K (depending on *Ln*), which seems to be related to a spin-state transition of the Co^{3+} ions [1,6,7,9,16–19].

Depending on the oxygen content, δ, several kinds of superstructures have been reported in the literature along with the various possible models of oxygen ordering [1–3,20,21]. The crystal structure adopted by $LnBaCo_2O_{5+\delta}$ has been reported to be tetragonal *P*4/*mmm* ($a_p \times a_p \times 2a_p$), orthorhombic *Pmmm* ($a_p \times 2a_p \times 2a_p$ or $a_p \times a_p \times 2a_p$), or orthorhombic *Pmmb* ($a_p \times 2a_p \times 2a_p$); where a_p refers to the simple cubic perovskite in the *Pm*-3*m* space group ($a_p \approx 3.9$ Å). The doubling of *c* is due to the ordering of *Ln* and Ba into layers perpendicular to *z*. The doubling of *b*, and the transition from tetragonal to orthorhombic, have been suggested to arise from an ordering of the oxide ion vacancies into channels at a value of $\delta = 0.5$ [1,3,6,21,22]. Due to the wide range of oxygen non-stoichiometry and a strong tendency of the oxygen ions and vacancies to order, the extra oxygen which is known to fill LnO_δ layers, can create complex crystal structures with mixed octahedral and pyramidal cobalt environments.

Several research groups have reported excellent properties of $LnBaCo_2O_{5+\delta}$ as cathode materials for intermediate temperature solid oxide fuel cells (IT-SOFCs) [23–25]. Our recent studies on $LnBa_{0.5}Sr_{0.5}Co_2O_{5+\delta}$ (*Ln*=Pr and Nd) show that the electrical conductivity decreases with temperature, and at 873 K the conductivity is 493 S/cm. Area specific resistance (ASR) decreases with increasing temperature, at 873 K the ASR is 0.286 Ωcm^2 [26].

The main objective of this work is to investigate the temperature dependent structural and magnetic properties in $PrBa_{0.5}Sr_{0.5}Co_2O_{5+\delta}$. The concise structural information was presented in our earlier publication [26]. Here we have explained structural data from Neutron Powder Diffraction (NPD) in detail and compared with the information from Specific Area Electron Diffraction (SAED). From the structural data, we have explored the oxygen content and mean valence states of Co at different temperatures (from RT to 973 K). We have also made the conductivity, thermogravimetric and magnetic measurements related with the structural data.

2. Experimental

Polycrystalline samples of $PrBa_{0.5}Sr_{0.5}Co_2O_{5+\delta}$ (PBSCO) were prepared by standard solid state reactions, starting with high purity oxides and carbonates (Pr_6O_{11}, Co_3O_4, $BaCO_3$, $SrCO_3$). The sample was fired in two steps. In the first step, the powders were mixed, pressed into pellets and heated in air at 1273 K for 8 h. The temperature was increased in 4 steps i.e. 423, 573, 773 and 973 K before reaching 1273 K. The duration of heating at each step was 2 h. The sample was then cooled down to room temperature, ground and ball milled for 24 h. In the second step, the sample was heated at 1373 K for 36 h. The heating and cooling rate was 5°/min for all cycles.

Phase purity, identity and homogeneity were confirmed by X-ray powder diffraction (XRD) experiments using a STOE Stadi P transmission diffractometer (Cu$K\alpha_1$, $\lambda = 0.15406$ nm). High resolution and high intensity time-of-flight NPD data were collected as a function of temperature using a GEM diffractometer at the ISIS spallation source at Rutherford Appleton Laboratory, UK. The sample (ca. 5 g) was loaded into a thin-walled, cylindrical vanadium can and placed in the sample chamber in ambient conditions. Neutron diffraction data was collected at 295, 373, 473, 573, 673, 773, 873 and 973 K using a furnace designed for the diffractometer. Rietveld analysis of the diffraction data sets were carried out using GSAS software [27]. The background was fitted using an empirical Chebyshev polynomial and peak shapes were considered as a pseudo-Voigt function. SAED patterns were collected on a Jeol JEM-2011 electron microscope operated at 200 kV. The powder sample was ground using a mortar and pestle, and suspended in acetone. One drop of suspension was deposited on a copper grid with a holey carbon film. Thermogravimetric analysis (TGA) was carried out on a NETZSCH TG 209 instrument to evaluate the oxygen content (weight loss) at different temperatures and to compare with neutron diffraction results. The initial weight of the sample was about 40 mg. The effect of buoyancy was corrected by using pre-empty crucible runs under the corresponding gas atmosphere and flow rates. The samples were heated up to 1073 K in the TG furnace at a heating rate of 5 K/min in air. The temperature dependent DC magnetization measurements were carried out in both field-cooled (FC) and zero-field-cooled (ZFC) modes, using a Quantum design PPMS in the temperature range 5 K to 300 K using magnetic fields 100 Oe, 500 Oe and 1000 Oe. Field dependent magnetisation data were collected from 0 Oe to 5000 Oe at 5 K.

3. Results and discussion

Rietveld refinement of room temperature (RT) XRD and NPD data shows that the structure can be refined using an average tetragonal symmetry with the unit cell parameters $a = b \approx a_p$ and $c \approx 2a_p$ and space group *P*4/*mmm* (No. 123). Careful investigation of the refined diffraction profile shows that in addition to this average structure a set of smaller unindexed peaks are present which is related to a superstructure. The most intense superstructure peak was observed at the *d*-spacing 4.468 Å and can be indexed as (1 1 1). These superstructure peaks are attributed to a particular order of oxygen vacancies in the structure and can be indexed by doubling both *a* and *b* lattice parameters. Different models and oxygen orderings were considered to explore the possible order arrangements of the oxygen vacancies. The first model corresponds to the orthorhombic symmetry in the space group *Pmmm* (No. 47) where *a, b* and *c* cell parameters are related as $a_p \times a_p \times 2a_p$. The second model was considered in the same space group with the relation $a_p \times 2a_p \times 2a_p$. Both the models were examined for different possibilities of oxygen ordering but no one of these were appropriate to explain the superstructure reflections. The third possibility corresponds to the *P*4/*mmm* space group in the setting $2a_p \times 2a_p \times 2a_p$ and with the perfect order in a $2a_p \times 2a_p$ supercell in the [PrO_δ] planes, with vacancies located in 1*b* (0 0 1/2), 1*d* (1/2 1/2 1/2) and 2*f* (0 1/2 0) Wyckoff positions. This model can also index superstructure reflections corresponding to the reflection condition HHL and HLL (H and L are odd numbers and $H \neq L$). The refinement of oxygen occupancies for other oxygen sites improved the peak intensity matching. It was observed from the refinement that the oxygen position at 1*d* (1/2 1/2 1/2) were completely vacant and 1*b* (0 0 1/2) and 2*f* (0 1/2 0) were partially vacant. Fig. 1a shows the Rietveld refinement profile and Table 1 shows the main crystallographic information of the room temperature NPD. The refinement of the structural parameters shows the possible ordering of oxygen vacancies and cations. The ordering of the oxygen vacancies in the perovskite matrix is responsible for the superstructure (also observed in the SAED pattern). The oxygen vacancies order within the [PrO_δ] layers, result in oxygen-rich and oxygen deficient *a*–*c* layers and consequently in a doubling of the unit cell along *a* and *b* directions [3]. The location of oxygen vacancies in [PrO_δ] planes does not correspond with the ordering into channels as reported for $LnBaCo_2O_{5.5}$ compounds [1]. Rietveld refinement of room temperature data shows the composition as $PrBa_{0.5}Sr_{0.5}Co_2O_{5.243}$. In this composition we have observed an imperfect order of the vacancies consisting in the preferential occupation of the 1*b* position. Partial disorder is restricted to a solution with atoms in 1*b* and 2*f* Wyckoff positions of the *P*4/*mmm* space group. In order

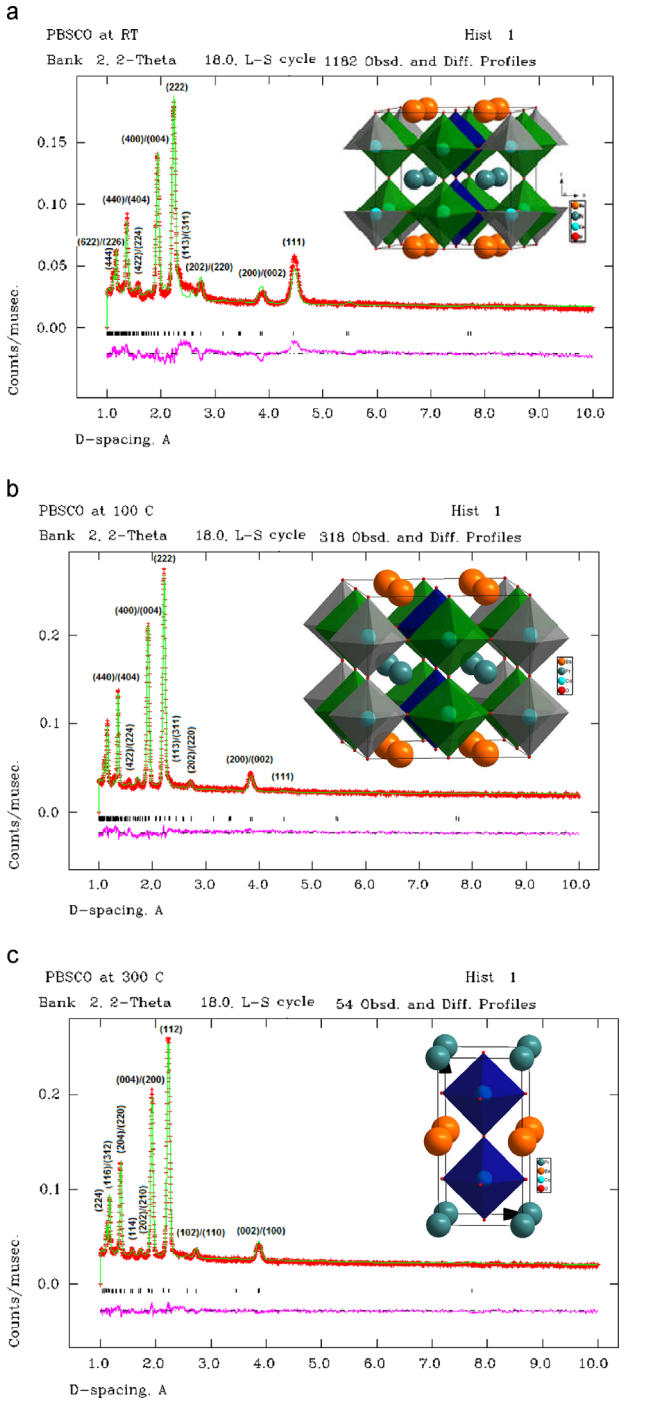

Fig. 1. (a) Observed (circles) and calculated (continuous line) NPD intensity profiles for $PrBa_{0.50}Sr_{0.5}Co_2O_{5.243}$ at RT in the *P4/mmm* space group where cell parameters are related as $2a_p \times 2a_p \times 2a_p$. The short vertical lines indicate the angular position of the allowed Bragg reflections. At the bottom in each figure the difference plot, $I_{obs} - I_{calc}$, is shown. Schematic 3D structure is shown in insert. (b) Observed (circles) and calculated (continuous line) NPD data Rietveld refinement profile for $PrBa_{0.50}Sr_{0.5}Co_2O_{5+\delta}$ at 373 K. Insert shows the schematic 3D structure. (c) Observed (circles) and calculated (continuous line) NPD data Rietveld refinement profile of $PrBa_{0.50}Sr_{0.5}Co_2O_{5+\delta}$ at 573 K in the *P4/mmm* space group where cell parameters are related as $a_p \times a_p \times 2a_p$. Insert shows the schematic 3D structure.

to get samples with perfect ordering (with all vacancies in 1*d* Wyckoff position only) it is important to make the samples in controlled manner to get an oxygen occupancy of 5.5.

The refinement of neutron diffraction data at 295, 373, 473, 573, 673, 773, 873 and 973 K shows that the ordering of oxygen vacancies exists from 295 K to 473 K. At 373 and 473 K, the intensity of the most intense superstructure reflection (1 1 1) was very low but other superstructure reflections like (1 1 3), (3 1 1) have small intensities. To match the intensities of these reflections it was important to consider the unit cell as $2a_p \times 2a_p \times 2a_p$. Fig. 1b shows the Rietveld refinement profile of NPD data collected at 373 K. In the temperature range 573 K to 973 K, the material shows the tetragonal symmetry in the *P4/mmm* space group with $a = b \approx a_p$ and $c \approx 2a_p$. Fig. 1c shows the Rietveld refinement profile of NPD data collected at 573 K. For the sake of simplicity the perfect order of the $2a_p \times 2a_p$ structure with 0% vacancy in 1*d* (1/2 1/2 1/2) and 2*f* (0 1/2 0) sites, and 100% vacancies in the 1*b* (0 0 1/2) sites are shown. Refined cell parameters, atomic positions, thermal parameters and atomic site occupancies at 295 K and 573 K are presented in Table 1(a) and (b). The unit cell parameters increase monotonically with temperature. The oxygen occupancy decreases with an increasing temperature. Bond valence sum calculations using the average ⟨Co–O⟩ bond distance shows that the three cobalt positions have different oxidation states at room temperature. For example, Co1 in the 2*g* (0 0 0.232) position has a mixed Co^{3+} and Co^{2+} state whereas Co2 and Co3 at 2*h* (1/2 1/2 *z*) and 4*i* (0 1/2 *z*) positions have oxidation states close to Co^{3+}. Selected bond lengths and calculated bond valence sums are given in Table 2 at 295 K, 473 K and 573 K. At 573 K, Co occupies only one position i.e. 2*h* (1/2 1/2 *z*) and is in Co^{3+} oxidation state.

SAED patterns revealed a $2 \times 2 \times 2$ superstructure in agreement with the NPD studies. The reported $a_p \times 2a_p \times 2a_p$ (space group *Pmmm*) for $PrBaCo_2O_{5+\delta}$ [22], $3a_p \times 3a_p \times 2a_p$ (space group *Pmmm*) for $HoBaCo_2O_{5.5}$ [1], $3\sqrt{2}a_p \times 3\sqrt{2}a_p \times 4a_p$ (space group *P4/mmm*) for$YBaCo_2O_{5.44}$ [28] were not observed in the present work. Fig. 2(a) and (b) shows a typical SAED pattern for $PrBa_{0.5}Sr_{0.5}Co_2O_{5+\delta}$ viewed down the [1 0 0] and [010] direction. The main phase can be indexed according to the cell parameters $a = 3.88$ ° and $c = 7.73$ ° from the *d*-spacings. The superstructure observed between a^* and b^*-axis indicates a doubling of the *a* and *b*-axes which is equal in the space group *P4/mmm*. In perovskites, the common superstructures are observed due to lattice distortion (or rotation of BO_6 octahedra) when the tolerance factor is smaller than 1. The superstructural dimensions in the *ab*-plane resulting from the rotation of octahedra are normally either $\sqrt{2}a_p \times \sqrt{2}a_p$ or $2a_p \times 2a_p$ [29,30]. $2 \times 2 \times 2$ superstructures can be derived from $1 \times 1 \times 2$ basic structures which develops from the ordering of oxygen vacancies. The $2 \times 2 \times 2$ superstructure in $PrBa_{0.5}Sr_{0.5}Co_2O_{5+\delta}$ is due to ordering of the extra oxygen in the Pr layer because this superstructure disappears when the extra oxygen anions are removed by heating the sample at high temperatures above 573 K.

Due to thermal expansion, the unit cell parameters *a* and *c* as well as unit cell volume increase with temperature after an initial drop from RT to 373 K. Fig. 3 shows the variation of unit cell parameters with temperature. Oxygen occupancy was increased from 295 K to 573 K and decreased from 573 K to 973 K. As mentioned above, during initial heating condition at low temperature ≥ 373 K, the vacant oxygen positions at 1*d* (1/2 1/2 1/2) created during synthesis become filled (see Fig. 1(a) and (b)). Above 373 K, these follow the normal behaviour to have more vacancies with increasing temperature. The total oxygen loss was about 0.25 O/f.u. This behaviour was strongly supported by the TGA data where we observed a weight gain below 373 K (Fig. 5). Fig. 4 shows the changes of oxygen occupancy and unit cell volume with temperature. Thermogravimetric analysis (TGA) in air shows a similar trend of weight loss; the weight loss due to the increasing oxygen deficiency from 573 K to 973 K was about 0.28 O/f.u. The initial weight increase in the temperature range RT to 573 K is supposed to be due to the oxygen vacancy filling in

Table 1
(a) Main crystallographic information for $PrBa_{0.5}Sr_{0.5}Co_2O_{5.243}$ (space group *P4/mmm*) from NPD data at room temperature in the $2a_p \times 2a_p \times 2a_p$ setting. The cell parameters, $a=7.7585(6)$ Å, $c=7.704(1)$ Å and the cell volume, $v=463.75(3)$ Å^3.

Atoms	Wyckoff position	*x*	*y*	*z*	*B*	Fractional occupancy
Pr	4*k* (*x x* 1/2)	0.2548(3)	0.2548(3)	0.5	0.011(2)	1.0
Ba/Sr	4*j* (*x x* 0)	0.2411(4)	0.2411(4)	0.0	0.003(7)	0.5/0.5
Co1	2*g* (0 0 *z*)	0.0	0.0	0.2323(3)	0.007(1)	1.0
Co2	2*h* (1/2 1/2 *z*)	0.5	0.5	0.319(2)	0.007(1)	1.0
Co3	4*i* (0 1/2 *z*)	0.0	0.5	0.2754(3)	0.007(1)	1.0
O1	1*a* (0 0 0)	0.0	0.0	0.0	0.001(8)	1.0
O2	1*c* (1/2 1/2 0)	0.5	0.5	0.0	0.004(7)	1.0
O3	2*f* (0 1/2 0)	0.0	0.5	0.0	0.020(4)	0.474(3)
O4	1*b* (0 0 1/2)	0.0	0.0	0.5	0.024(2)	0.024(5)
O5	2*e* (0 1/2 1/2)	0.0	0.5	0.5	0.010(7)	1.0
O6	8*s* (*x* 0 *z*)	0.2616(4)	0.0	0.2773(3)	0.052(3)	1.0
O7	8*t* (*x* 1/2 *z*)	0.2585(4)	0.5	0.2444(4)	0.043(5)	1.0
(b) Main crystallographic information for $PrBa_{0.5}Sr_{0.5}Co_2O_{5+\delta}$ (space group *P4/mmm*) from NPD data at 573 K in the $a_p \times a_p \times 2a_p$ setting. The cell parameters, $a=3.8852(3)$ Å, $c=7.729(1)$ Å and the cell volume, $v=114.871(5)$ Å^3.						
Pr	1*a* (0 0 0)	0.0	0.0	0.0	0.008(1)	1.0
Ba/Sr	1*b* (1/2 0 0)	0.5	0.0	0.0	0.018(5)	0.5/0.5
Co	2*h* (1/2 1/2 *z*)	0.0	0.0	0.2452(3)	0.009(7)	1.0
O1	1*c* (1/2 1/2 0)	0.5	0.5	0.0	0.001(7)	0.9534
O2	1*d* (1/2 1/2 0)	0.5	0.5	0.5	0.011(3)	1.0
O3	4*i* (1/2 0 *z*)	0.5	0.0	0.2433(2)	0.030(6)	0.9469

Table 2
Main bond distances (Å) ($d \leq 3.5$ Å) and bond valence sums (BVS) for $PrBa_{0.5}Sr_{0.5}Co_2O_{5+\delta}$ determined from NPD data at RT, 473 K and 573 K.

Parameters	RT	200 °C	Parameters	300 °C
$Co1–O_6$ Octahedra			$Co–O_6$ Octahedra	
Co1–O1 (Å) (× 1)	1.7899(2)	1.8877(2)	Co–O1(× 1)	1.8949(3)
Co1–O4 (Å) (× 1)	2.0622(3)	1.9647(2)	Co–O2(× 1)	1.9695(3)
Co1–O7 (Å) (× 4)	2.0588(1)	2.0915(2)	Co–O3(× 4)	1.9276(2)
⟨Co1–O⟩(Å)	2.0145(2)	2.036(4)	⟨Co–O⟩ (Å)	1.9291(3)
Bond valence sum	2.43	2.29	*Bond valence sum*	3.06
$Co2–O_6$ Octahedra		PrO_{12} Polyhedra		
Co2–O2 (Å) (× 1)	2.4576(3)	2.5272(4)	Pr–O1(× 4)	2.7260(2)
Co2–O5 (Å) (× 1)	1.3946(2)	1.3252(4)	Pr–O3(× 8)	2.6930(2)
Co2–O8 (Å) (× 4)	1.9588(2)	1.9993(2)		
⟨Co2–O⟩ (Å)	1.9479(2)	1.9749(3)		
Bond valence sum	2.91	2.71		
$Co3–O_6$ Octahedra				
Co3–O3 (Å) (× 1)	2.1220(3)	1.5140(3)		
Co3–O6 (Å) (× 1)	1.7302(2)	2.3384(4)		
Co3–O7 (Å) (× 2)	1.8498(1)	2.0241(2)		
Co3–O8 (Å) (× 2)	2.0193(2)	2.0122(2)		
⟨Co3–O⟩ (Å)	1.9317(2)	1.9875(3)		
Bond valence sum	3.04	2.62		

the structure. Fig. 5 shows the TGA plot from 298 K to 1073 K collected in air. TGA results on heating in flowing air shows an initial apparent weight gain up to 373 K and then a weight loss due to buoyancy drift or possibly water desorption. A small weight grain from TGA results is observed in the vicinity of 573 K when the sample re-equilibrates gaining oxygen from the atmosphere and then a decrease as the equilibrium oxygen content decreases with temperature.

The electrical conductivity decrease with increasing temperature suggests a metallic behaviour. The apparent metallic conductivity behaviour may relate to an energy band overlap between Co-3d and O-2p and the presence of Co^{4+} ions from thermally generated charge disproportion of Co^{3+} [22,26,31]. The weight loss in TGA starts at 573 K which is well above where the maximum conductivity was observed. This indicates that this maximum relates to an insulator to metal transition on heating, that can be electrically or magnetically driven, and seems likely to be similar to the electronic orbital ordering transition leading to metal-insulator transition observed in the related phases $SmBaCo_2O_{5+\delta}$ [23], $YBaCo_2O_{5+\delta}$ [2] and $GdBaCo_2O_{5.5}$ [32]. The observed ASR value was 0.153 Ω cm^2 at 973 K and 0.286 Ω cm^2 at 923 K [26] which is better than the value of 0.602 Ω cm^2 at 923 K for GBCO reported by Chang et al. [11]. The activation energy of PBSCO was 1.07 eV which is also lower than the activation energy found for GBCO (1.34 eV). The low value of ASR and activation energy is related to the fast oxygen diffusion in the bulk and high kinetics on the surface of the electrode [12].

Fig. 6 shows the temperature dependence of the dc magnetization of $PrBa_{0.5}Sr_{0.5}Co_2O_{5.243}$ in ZFC and FC condition, and the inverse susceptibility data under the applied field of 100, 500 and 1000 Oe after a field cooling process. In ZFC measurements at 100 Oe, the value of magnetisation increases with temperature and shows a maximum at 192(1) K just before a sharp decrease, this is due to an antiferromagnetic (AFM) transition (Fig. 6(a)). In higher magnetic fields i.e. at 500 Oe and 1000 Oe, the sharp transition changes to a broad maximum and decreases the transition temperatures (Fig. 6(b) and (c)). In FC measurements at 100 Oe, magnetisation decreases with increasing temperature which indicates a ferromagnetic (FM) transition. At around 210 K, a sudden decrease of magnetisation was observed which indicates the transition of the ferromagnetic phase to a paramagnetic phase. The FM to PM transition temperature as well as the value of magnetisation increases with magnetic field. At 100, 500 and 1000 Oe magnetic fields, the values of T_c were 210.10(2), 214.20(2) and 219.30(3) K. From the inverse susceptibility of the ZFC curve, T_N is found to be 52(2) K. At 4.00 K, the magnetisation values were 7.33, 18.30, 22.12 emu/g for 100, 500 and 1000 Oe magnetic fields, respectively. This $M(T)$ evolution clearly differs from that in $PrBaCo_2O_{5.76}$ and $PrBaCo_2O_{5.74}$ where FC curves shows AFM to FM to PM transitions [3]. This behaviour is also different from $RBaCo_2O_{5.5}$ compounds, where a maximum around 250 K is followed by a deep and abrupt drop of the magnetisation at 40–60 K below the first enhancement [18]. $PrBaCo_2O_{5+\delta}$ show different types of magnetic ordering depending on the oxygen content. Oxygen ordering has a strong effect on the magnetic properties of this compound. The magnetic properties are extremely sensitive in the $\delta \sim 0.5$ region. An antiferromagnetic state was found for $\delta < 0.35$. For $\delta = 0.35–0.7$, a cluster glass state was observed where oxygen-poor and oxygen-rich clusters coexist

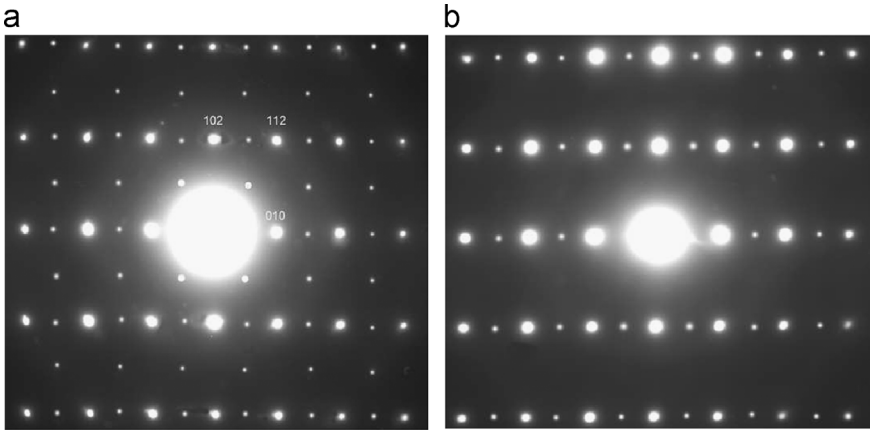

Fig. 2. SAED pattern of solid solution of $PrBa_{0.50}Sr_{0.5}Co_2O_{5+\delta}$ at RT viewed down the [1 0 0] zone axis.

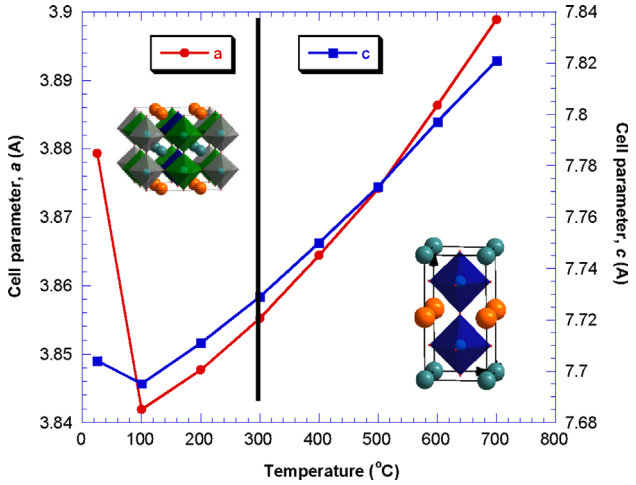

Fig. 3. Plot of unit cell parameters *a* and *c* versus temperature.

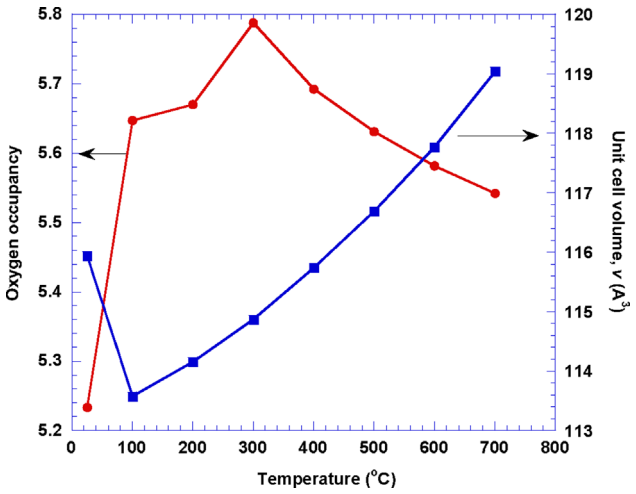

Fig. 4. Change of oxygen occupancy and unit cell volume with temperature.

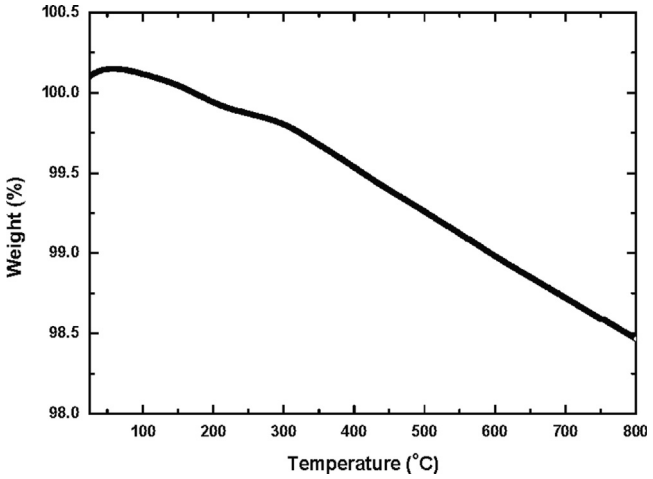

Fig. 5. TGA plot of $PrBa_{0.50}Sr_{0.5}Co_2O_{5+\delta}$ on heating from 298 K to 1073 K in air.

[22]. The reciprocal susceptibility versus temperature has been plotted for all magnetic fields (Fig. 6(a)–(c)). The $\chi^{-1}(T)$ curves exhibit an abrupt drop in χ^{-1} as T decreases. At high temperatures χ^{-1} for FC and ZFC coincide but at low temperatures below 200 K the inverse susceptibility of ZFC increases whereas inverse susceptibility of FC remains constant. This phenomenon also suggests the existence of AFM state.

The isothermal magnetic hysteresis curve shown in Fig. 7 has been recorded at 5 K after zero-field-cooling from room temperature. The first magnetization curve show the usual step followed by a quick rise of the magnetic moment. The field at which the quick rise starts was about 1 kOe which is similar to the composition $PrBaCo_2O_{5.74}$ [3]. At this temperature the magnetizing process is highly irreversible. The hysteresis curve shows the saturation magnetization is 26 emu/g, remanence magnetization is 20 emu/g and the coercive field is 180 Oe. This hysteresis behaviour, especially remanent magnetization, is indicative of a FM transition. This hysteresis behaviour is different from the M(H) behaviour of $RBaCo_2O_{5.5}$ in the AFM phase where a field-induced FM moment occurs at higher critical fields and the transition has been related to the spin alignment of AF-coupled adjacent FM ladders with Ising like anisotropy [18,33]. For $T \ll T_{cusp}$ the $M(H)$ curves are straight lines with a weak hysteresis in good indication of antiferromagnetism. As shown in Fig. 6(a)–(c), the FM clusters grow as a function of applied field. The existence of AFM at low temperature was confirmed by zero-field-cooled neutron diffraction in $PrBaCo_2O_{5+\delta}$ [3].

In spite of similarities in the magnetic behaviour, we have observed a number of differences from Sr-free compositions. The value of the FM and AFM components at low temperature, the coercive field, remanent magnetization, Néel and Curie temperature were different. These discrepancies are related to the oxygen

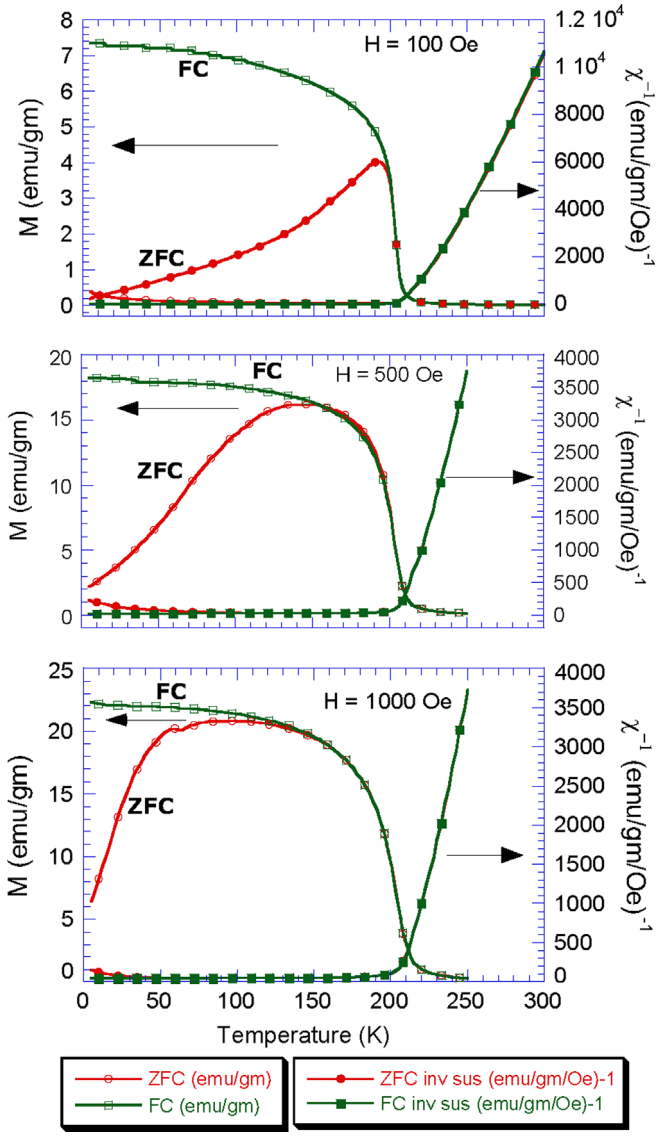

Fig. 6. Magnetisation versus temperature plot measured at different field i.e. 100 Oe (a), 500 Oe (b) and 1000 Oe (c). Right hand side *y*-axis shows the inverse susceptibility versus temperature curves.

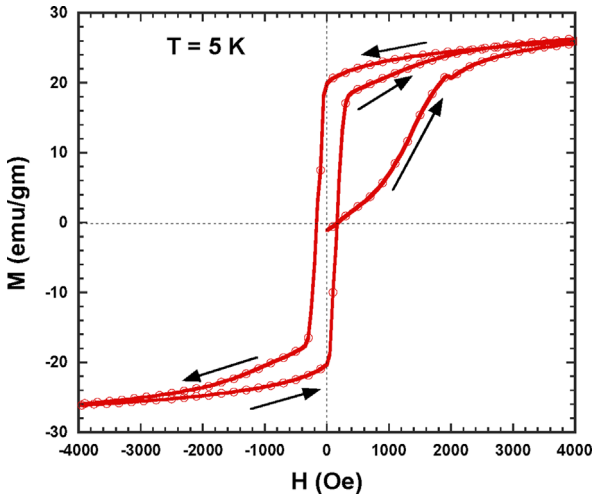

Fig. 7. Magnetisation versus magnetic field plot at 5 K.

content and the degree of vacancy ordering. A Sr-doped sample shows higher FM and lower AFM transition at lower oxygen content. The oxygen content and the vacancy ordering govern the magnetic interactions. A decrease of the degree of order drives a decrease of the AFM strength leading to a decrease of Néel temperature. The magnetic order consists of a canted AFM G-type structure and do not overlap with FM. For $T < T_{cusp}$ the FC and ZFC curves can merge only at a high magnetic field. Both kinds of $M(H)$ and $M(T)$ curves demonstrate that ferromagnetism develops in the T_{cusp} vicinity. The existence of a ferromagnetic component in a narrow range of temperature is a possible canting of the spin between cobalt in fivefold and six-fold coordinations and the component can thus be viewed as ferromagnetic below 210 K. High spin Co^{3+} and low spin Co^{4+} ions occupy the octahedral and intermediate spin Co^{3+} occupy the pyramids [3].

4. Conclusions

$PrBa_{0.5}Sr_{0.5}Co_2O_{5+\delta}$ has been synthesised and characterized, with $\delta = 0.234$. From XRD and NPD data we have found that the most likely distribution of oxygen vacancies is in the PrO_δ planes corresponding to an imperfect order in which the vacancies are inhomogeneously distributed. At RT it forms a $2 \times 2 \times 2$ superstructure based on the ordering of these vacancies. The structure was found to be tetragonal in the *P*4/*mmm* space group. SAED patterns confirm the superstructure reflections and the doubling of *a* and *b* axis. Above 573 K, the unit cell can be defined as $a = b \approx a_p$, $c \approx 2a_p$. Oxygen occupancy increases from RT to 373 K and then decreases with increasing temperature which was supported by the initial weight gain in TGA data. Temperature evolution neutron diffraction and thermogravimetric analysis measurements show that at 973 K the total oxygen loss is about 0.265 O/formula unit. Electrical conductivity measurements in air show a metallic behaviour. Magnetization data show that, on cooling, the samples show a paramagnetic-to-ferromagnetic transition in the field cooled condition and paramagnetic-to-antiferromagnetic transition in the zero field condition. This indicates the coexistence of FM and AFM ordered states where the FM state is dominant. Hysteresis measurements confirm the ferromagnetic state and show 20 emu/g (approximately) remanent magnetisation at 5 K.

Acknowledgments

The authors are grateful for the financial support given by the Engineering and Physical Sciences Research Council (EPSRC) in United Kingdom. One of the authors, J.H. Kim is grateful for the support from the new and renewable energy (Diesel desulfurization for 300 kW MCFCs) of the Korea Institute of Energy Technology Evaluation and Planning (KETEP) grant funded by the Korea Government Ministry of Knowledge and Economy (MKE). The authors are also thankful to Dr. David Miller for his help during SAED measurements and Dr Martin Blundell for discussions. JI thanks the Royal Society for a Wolfson Merit Award.

References

[1] A. Maignan, C. Martin, D. Pelloquin, N. Nguyen, B. Raveau, J. Solid State Chem. 142 (1999) 247.
[2] A. McKinlay, P. Connor, J.T.S. Irvine, W. Zhou, J. Phys. Chem. C 111 (51) (2007) 19120.
[3] C. Frontera, J.L. Gacia-Munoz, A.E. Carrillo, C. Ritter, D.M. Marero, A. Caneiro, Phys. Rev. B: Condens. Matter 70 (2004) 184428.
[4] T. Vogt, P.M. Woodword, P. Karen, B.A. Hunter, P. Henning, A.R. Moodenbaugh, Phys. Rev. Lett. 84 (2000) 2969.
[5] E. Surad, F. Fauth, V. Caignaert, I. Mirebeau, G. Baldinozzi, Phys. Rev. B: Condens. Matter 61 (2000) (R 11871).

[6] Y. Moritomo, T. Akimoto, M. Takeo, A. Machida, E. Nishibori, M. Takata, M. Sakata, K. Ohoyama, A. Nakamura, Phys. Rev. B: Condens. Matter 61 (2000) (R13 325).
[7] C. Frontera, J.L. Garcia-Munoz, A. Llobet, M.A.G. Aranda, Phys. Rev. B: Condens. Matter. 65 (2002) 180405.
[8] F. Fauth, E. Surad, V. Caignaert, I. Mirebeau, Phys. Rev. B: Condens. Matter 66 (2002) 184421.
[9] A.A. Taskin, A.N. Lavrov, Y. Ando, Phys. Rev. Lett. 90 (2003) 227201.
[10] A.A. Taskin, A.N. Lavrov, Y. Ando, Appl. Phys. Lett. 86 (2005) 091910.
[11] A. Chang, S.J. Skinner, J.A. Kilner, Solid State Ionics 177 (2006) 2009.
[12] G. Kim, S. Wang, A.J. Jacobson, L. Reimus, P. Brodersen, C.A. Mims, J. Mater. Chem. 17 (2007) 2500.
[13] A.Yu. Suntsov, I.A. Leonidov, M.V. Patrakeev, V.L. Kozhevnikov, J. Solid State Chem. 206 (2013) 99.
[14] D. Akahoshi, Y. Ueda, J. Solid State Chem. 156 (2001) 355.
[15] J.F. Mitchell, J. Burley, S. Short, J. Appl. Phys. 93 (2003) 7364.
[16] D.D. Khalyavin, S.N. Barilo, S.V. Shiyacv, G.L. Bynchkov, I.O. Troyanchuk, A. Furrer, A. Allenspach, H. Szymczak, R. Szymczak, Phys. Rev. B: Condens. Matter 67 (2003) 214421.
[17] C. Martin, A. Maignan, D. Pelloquin, N. Nyguen, B. Raveau, Appl. Phys. Lett. 71 (1997) 1421.
[18] O.I. Troyanchuk, N.V. Kasper, D.D. Khalyavin, H. Szymczak, R. Szymczak, M. Baran, Phys. Rev. Lett. 80 (1998) 3380.
[19] A. Maignan, V. Caigneart, B. Raveau, D. Khomskii, G. Swatzsky, Phys. Rev. Lett. 93 (2004) 026401.
[20] W. Zhou, Chem. Mater 6 (1994) 441.
[21] J.C. Burley, J.F. Mitchell, S. Short, D. Miller, Y. Tang, J. Solid State Chem. 170 (2003) 339.
[22] S. Streule, A. Podlesnyak, J. Mesot, M. Medarde, K. Conder, E. Pomjakushina, E. Mitberg, V. Kozhevnikov, J. Phys. Condens. Matter 17 (2005) 3317.
[23] J.-H. Kim, Y. Kim, P.A. Connor, J.T.S. Irvine, J. Bae, W. Zhou, J. Power Sources 194 (2009) 704.
[24] J.-H. Kim, A. Manthirama, J. Electrochem. Soc. 155 (2008) B385.
[25] J.H. Kim, M. Cassidy, J.T.S. Irvine, J. Bae, J. Electrochem. Soc. 156 (2009) B682.
[26] A.K. Azad, J.H. Kim, J.T.S. Irvine, J. Power Sources 196 (2011) 7333.
[27] A.C. Larson, R.B.V. Dreele, Technical Report LANSCE, MSH805, Los Alamos National Laboratory, 1985.
[28] D.D. Khalyavin, D.N. Argyriou, U. Amann, A.A. Yaremchenko, V.V. Kharton, Phys. Rev. B: Condens. Matter 75 (2007) 134407.
[29] A.C. Mclaughlin, J.P. Attfield, R.S. Liu, L.Y. Jang, W.Z. Zhou, J. Solid State Chem. 177 (2004) 834.
[30] A.M. Kusainova, P. Lightfoot, W.Z. Zhou, S. Yu., A.O. Stenfannovich, V. A. Mosunov, Chem. Mater. 13 (2001) 4731.
[31] J.W. Moon, Y. Masuda, W.S. Seo, K. Koumoto, Mater. Sci. Eng., B 85 (2001) 70.
[32] C. Frontera, J.L. Garcia-Munoz, A. Llobet, M.A.G. Aranda, J. Rodriguez-Carvajal, M. Respaud, J.M. Broto, B. Raquet, H. Rakoto, M. Goiran, J. Alloys Compd 468 (2001) 323.
[33] M. Respaud, C. Frontera, J.L. Garcia-Munoz, M.A.G. Aranda, B. Raquet, J. M. Broto, Phys. Rev. B: Condens. Matter 64 (2001) 214401.